Modelling, Simulation and Stability of Free Surface and Bulk Nanobubbles in Hydrogen Electrolysis

Sven-Joachim Kimmerle *

* *University of the German Federal Armed Forces Munich, Institute of Mathematics and Computer Applications (LRT-1), 85577 Neubiberg/München, Werner-Heisenberg-Weg 39, Germany (e-mail: sven-joachim.kimmerle@unibw.de)*

Abstract: We consider two examples for precipitation by phase transitions, nanobubbles arising in hydrogen electrolysis, using polymer electrolyte membrane electrolysers, and liquid arsenic rich droplets in gallium arsenide crystals. We present the modelling and derive macroscopic evolution equations by formal homogenization techniques exploiting typical scales. The resulting dynamical systems are simulated. We discuss stationary solutions and their stability. This allows to validate our models.

Keywords: Free boundary problem, Nonlinear dynamical system, Formal homogenization, Mean field model, Phase transition, Precipitation, Hydrogen electrolysis, Surface nanobubbles, Gallium arsenide, Stability

1. MODEL PROBLEMS

Precipitates, i.e. domains of a new phase within another phase, arise in many applications in science and engineering. Usually in precipitation, the domains of the new phase are small and disconnected, but many bubbles (gas), droplets (liquid), or inclusions (solid) are encountered within the surrounding connected phase. In this paper we focus on the time evolution of precipitates, in particular stationary solutions and their stability.

As first example we consider hydrogen nanobubbles that are produced within polymer electrolyte membrane (PEM) electrolysers. The goal of this process is to split water by electric energy, e.g. provided by photovoltaic devices, into hydrogen and oxygen:

$$2\,H_2O \rightleftharpoons O_2 + 4\,H^+ + 4\,e^- \rightleftharpoons O_2 + 2\,H_2. \qquad (1)$$

As a side effect, this could allow for storing fluctuant renewable energies in the form of hydrogen, avoiding unnecessary energy losses. The hydrogen may be used for proton exchange membrane fuel cells (PEMFC), converting hydrogen and oxygen (e.g. from air) into electrical energy and, as byproduct, water. It is a tempting idea to employ for the hydrogen electrolysis again the hydrogen PEMFC. Hydrogen could be liquified under high pressures and may serve as an energy carrier, but the cost of hydrogen production needs to be reduced for this technology being cost-effective. Today, the most widespread method for producing hydrogen is steam reforming from methane, electrolysis might be a green alternative.

Within electrolysis, the typically high concentrations of hydrogen lead inevitably to precipitation of gaseous bubbles. Small nanobubbles appear at the surface of the cathode (negative within electrolytic mode of operation), then detach and become suspended spherical nanobubbles within water (Seddon et al. (2012)). As an unwanted effect the generation of surface nanobubbles covers increasingly the platinum (Pt) part of the electrode and might hinder hydrogen production there. For electrolysis, the goal is to achieve a stable hydrogen flux away from the cathode, i.e. a regime of stable surface and bulk nanobubbles. To the knowledge of the author, there is no good understanding of the long-life properties of nanobubbles (Zhang et al. (2008); Luo et al. (2013)). According to classical theory it is expected that nanobubbles dissolve within microseconds, however life-times of $10^{-2} - 10^{-1}$s are observed in experiments. Our model suggests an explanation for this phenomenon.

Another example is the precipitation of arsenic (As) rich liquid droplets within a gallium arsenide (GaAs) crystal. At the end of the production process of semi-insulating GaAs wavers, a final heat treatment is applied in order to ameliorate certain properties of the semi-insulator. However, liquid droplets may nucleate and shrink or grow further. The droplets may be assumed to be spherical, their chemical potential is largely influenced by surface tension, but mechanical bulk stresses within the crystal have to be taken into account, too (Dreyer et al. (2008)). The goal is to limit the growth and to obtain a homogeneous distribution in order not to destroy the semi-insulating properties of the crystal (Kimmerle (2013)).

2. MATHEMATICAL METHODS

Precipitation processes can be modelled mathematically as free boundary problems. Free boundary problems are described by different approaches. The phases may be modelled on an atomic level, where one considers the balance of atom/molecule numbers, or on a continuum level. Within continuous models one can model the phase interface as a mushy region, as it is done in phase field models (also called diffuse-interface models), or by sharp interface mod-

els, as e.g. the Mullins Sekerka model. The different models correspond to different mathematical methods: Phase-field models may be solved be level set methods, sharp-interface models could be treated by transformation techniques. For free contact boundaries, variational inequalities or complementarity conditions, are another option. In many situations, the motion of the sharp interface is either dominated by volume diffusion or by interface reactions, yielding different free boundary conditions (Stefan conditions) for each regime. In general, we are not primarily interested in solving for the precise evolution of every precipitate, but in macroscopic quantities, like the volume fraction of precipitates or the long-time behaviour. For this purpose, continuum as well as atomic models may be considered through the glasses of a homogenization method. A classical macroscopic model is the LSW model, due to Lifshitz-Slyozov and Wagner, that is derived e.g. within the limit of vanishing precipitate fraction from the Mullins-Sekerka model, see e.g. Niethammer et al. (2001).
In this paper we work with a sharp-interface model, where the evolution of the interface is given by a further differential equation for the free boundary. We only consider the volume-diffusion controlled (DC) regime.

3. NANOBUBBLES IN HYDROGEN ELECTROLYSIS

3.1 Modelling precipitation

In our model we assume a constant temperature and constant outer pressure. Hydrogen surface nanobubbles can be described as spherical caps sitting at the solid/liquid interface, for typical dimensions see table 1. In addition, micropancakes with a height of $1-2\,\mathrm{nm}$ and radii of $100-900\,\mathrm{nm}$ are observed at the solid/liquid interface (Seddon et al. (2012)). Furthermore, we encounter suspended spherical nanobubbles in the liquid. We emphasize that we say spherical bubble or (nano)sphere and surface bubble or (nano)cap, whereas bubble or precipitate comprises all three types. As a first validation approach we will only consider nanospheres and nanocaps in this study.
For the geometry, we consider a box domain $Q := [-\ell,\ell]^2 \times [0,2\ell] \subset \mathbb{R}^3$ with the electrode as one (flat) boundary $\Sigma := \{x \in Q \,|\, x_3 = 0\}$, the top boundary $Z := \{x \in Q \,|\, x_3 = 2\ell\}$, and the remaining side boundaries Π. Q has several, let's say $\mathcal{N} \in \mathbb{N}_*$, gaseous inclusions (bubbles) $G^{(i)}$, being several nanocaps $C^{(i)}$ and several spherical nanobubbles $S^{(i)}$. In the following the upper indices (i) refer to the corresponding sphere or cap, i running from $1,\dots\mathcal{N}$. The gas phase (hydrogen) is represented by $G = \cup_{i=1}^{\mathcal{N}} G^{(i)}$ and the liquid phase (protonated water) by $L = Q \setminus \overline{G}$, $\overline{G}$ denoting here the closure of G. $I^{(i)} = \partial G^{(i)} \cap \partial L$ denotes the gas-liquid phase interfaces.
The assumptions of spherical bubbles and spherical caps are consistent with a hydrogen concentration c_l/c_g, in liquid/gas respectively, both constant on the respective side of an interface. In the DC regime the motion of each interface is driven by the jump of diffusion flux j at the interface, see (7) below. The $\mathcal{N}_s$ nanospheres are parametrized by their radii $\mathcal{R}^{(i)}$. We characterize the $\mathcal{N}_c = \mathcal{N} - \mathcal{N}_s$ spherical caps by their curvature radius $\mathcal{R}^{(i)}$, see Fig. 1. W.l.o.g. we may order the bubbles by type, starting with nanospheres, $i = 1,\dots,\mathcal{N}_s$ and then we list the radii of the nanocaps with indices $i = \mathcal{N}_s+1,\dots,\mathcal{N}$. Let $\Theta^{(i)}$ denote the angle between flat surface and the tangential plane to the spherical cap, see Fig. 1. The (half-)width of the cap follows as $a^{(i)} = \mathcal{R}^{(i)} \sin\Theta^{(i)}$. For an overview of typical quantities and their values see table 1.

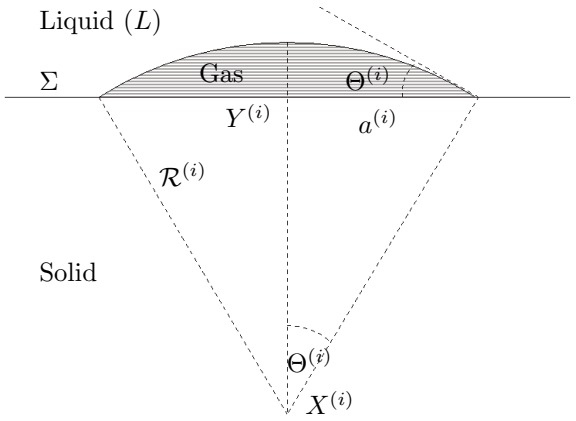

Fig. 1. Cross section of a spherical surface nanocap (shaded) on a flat surface.

Spheres and caps may grow or shrink and, possibly, dissolve when for the first time $\mathcal{R}^{(i)} \le 0$ and then the precipitate is taken out of the balance equations. Note that we do not consider nucleation of new precipitates within this model. Therefore the numbers $\mathcal{N}$, $\mathcal{N}_c$ and $\mathcal{N}_s$ will also depend on time. Let $X^{(i)}$ denote the centers of the curvature spheres, that are fixed in case of nanospheres. For caps the centers of the curvature sphere are a technical construction: They lie outside Q and may move, but their orthogonal projection onto Σ, the center $Y^{(i)}$ of the contact circle, remains fixed.
The interfaces may be parametrized by the radii, $I^{(i)} = \partial B_{\mathcal{R}^{(i)}}(X^{(i)}) \cap Q$. The initial geometry is prescribed by $\mathcal{R}^{(i)}(0) = \mathcal{R}_0^{(i)}$, $\Theta^{(i)}(0) = \Theta_0^{(i)}$, $\mathcal{N}_s(0) = \mathcal{N}_s^0$, $\mathcal{N}_c(0) = \mathcal{N}_c^0$, and $\mathcal{N}(0) = \mathcal{N}^0$ with given $\mathcal{R}_0^{(i)} > 0, \Theta_0^{(i)} \in (0,\pi), \mathcal{N}_s^0, \mathcal{N}_c^0 \in \mathbb{N}_*$. We consider the precipitate evolution for times t in a finite time interval $[0,\mathcal{T}]$.
Let c denote the unknown (non-negative) concentration of hydrogen, p the pressure, and D the given diffusion coefficient. Quantities like c, p, or D are restricted to a certain phase by subindices l for liquid or g for gas, since the may jump at the phase interface. In the liquid and in the gas phase Fick's law holds,

$$j = -D\nabla c \quad \text{in } Q \setminus \cup_{i=1}^{\mathcal{N}} I^{(i)}, \tag{2}$$

with the quasi-static diffusion equation $\nabla \cdot j = 0$ we find

$$\nabla \cdot (D\nabla c) = 0 \quad \text{in } Q \setminus \cup_{i=1}^{\mathcal{N}} I^{(i)}, \tag{3}$$

that simplifies to the Laplace equation, since we assume a constant diffusion coefficient D in each phase, respectively. This yields directly with the assumption of spherical

Quantity	Symbol	Value	Unit
Length electrode segment	ℓ	1	μm
Typical radii (spheres)	$\mathcal{R}^{(i)}$	$100-1000$	nm
Typical widths (caps)	$a^{(i)}$	$50-100$	nm
Typical temperature	T	298	K
Diff. coefficient (liquid)	D_l	$7.0\cdot10^{-10}$	m^2/s
Henry constant	H	$1.91\cdot10^{-2}$	1
Surface tension H_2O/H_2	γ	0.07	N/m
Equilibr. saturation conc. H	$\hat{c}_l^{eq}$	0.8	$\mathrm{mol}/\mathrm{m}^3$

Table 1. Experimental data (Luo et al. (2013))

droplets, that $c_g^{(i)}$ is constant in space within each bubble. Let R denote the gas constant and T the temperature. According to the ideal gas law, we have for the gas pressure $p_g^{(i)}$, consisting of hydrogen only, the constant value $p_g^{(i)} = RTn_g^{(i)}/V^{(i)} = RTc_g^{(i)}$, $n_g^{(i)}$ denoting the number density of hydrogen molecules in the bubble i with volume $V^{(i)}$. Then the Young-Laplace law yields for the pressure difference between the liquid pressure $p_l^{(i)}$ at the inferface $I^{(i)}$ and the pressure $p_g^{(i)}$ in bubble i

$$RTc_g^{(i)} = p_g^{(i)} = p_l^{(i)} + 2\gamma/\mathcal{R}^{(i)}, \tag{4}$$

where γ is the surface tension, assumed to be constant. We write $c_l^{(i)} = c_l|_{I^{(i)}}$. Note that according to a model for charged fluid flow in PEM (Novruzi et al. (2014)) in case of small fluid flows, we have the following law (formally similar to the ideal gas law) in the liquid $p_l^{(i)} = RTc_l^{(i)} + p_{\mathrm{H_2O}}$, where the partial pressure $p_{\mathrm{H_2O}}$ of water turns out to be neglible.

In principle, $\Theta^{(i)}$ has to be determined. Classically, one determines the contact angle via the Young-Dupré equation, a relation of the surface tensions/energies, $\gamma_{sl} - \gamma_{sg} - \gamma\cos\Theta^{(i)} = 0$, where γ_{sl} and γ_{sg} are the interfacial energies between solid/liquid and solid/gas, resp. Unfortunately, measurements of the latter are not available in literature for our situation, as far as to the knowledge of the author. We assume $\Theta^{(i)} = 5^\circ = const$, corresponding to radii of curvature for caps between $100 - 1000$ nm. In general, γ_{sl}, γ_{sg}, and thus $\Theta^{(i)}$ might depend on $\mathcal{R}^{(i)}$. The volume of a sphere is well-known, for the surface cap we have $(4\pi/3)(\mathcal{R}^{(i)})^3\omega$, where we abbreviate $\omega := (1 - \cos\Theta^{(i)})^2(2 + \cos\Theta^{(i)})/4$.

We have to determine the hydrogen concentration $c_l^{(i)}$ in the solute at the interface $I^{(i)}$. The Henry law relates the partial pressure $p_{\mathrm{H_2}}$ of hydrogen to the equilibrium concentration $\hat{c}_l$ of the solute by $p_{\mathrm{H_2}} = H\hat{c}_l/\hat{c}_g$, where H is the dimensionless version of the Henry constant, yielding (by means of a Taylor expansion around the equilibrium) the local flux between a bubble and the liquid (Sperre (2014)), $j|_{I^{(i)}} \approx \alpha(c_l^{(i)} - Hc_g^{(i)})\nu$, α being a proportionality constant, ν the outer normal. In case of zero net flux we have

$$c_l^{(i)} = Hc_g^{(i)}. \tag{5}$$

In Sperre (2014) a dynamic equilibrium for one bubble is considered. A surface nanobubble can be in dynamical equilibrium by steady in- and outflux over the bubble interface, since the gas concentration is higher at a hydrophobic wall, yielding an influx into the bubble, than at the top of the cap (just liquid), where the outflux takes place. In this situation the Henry law only holds for concentration averages over the interface. In contrary, we will consider a quasi-static equilibrium that is obtained by interaction of the hydrogen bubbles through a mean hydrogen concentration in the solute. Therefore we combine the Henry law with (4) and get

$$c_g^{(i)} = \sigma/(H\mathcal{R}^{(i)}), \qquad c_l^{(i)} = \sigma/\mathcal{R}^{(i)}, \tag{6}$$

where we introduce $\sigma = 2\gamma H/(RT(1-H))$ for brevity.

We emphasize that we assume that the bubbles consist only of hydrogen. By conservation of substance we motivate the following free boundary condition, see Dreyer et al. (2008); Kimmerle (2009),

$$\frac{\partial}{\partial t}\mathcal{R}^{(i)} = \frac{[j]_g^l \cdot \nu}{\mathbb{X}[c]_g^l} = -\frac{\nabla(D_l c_l^{(i)} - D_g c_g^{(i)}) \cdot \nu}{\mathbb{X}(c_l^{(i)} - c_g^{(i)})}, \tag{7}$$

where the jumps $[\cdot]$ are from liquid to gas. For simplicity, we approximate here the function $\mathbb{X}$ by 1. This so-called Stefan condition determines the radii evolution.

It remains to determine the boundary conditions (b.c.) for c_l. At the flat electrode surface outside the droplets we have a given influx j_{in} of hydrogen, that is produced at the electrode

$$-D_l\nabla c_l \cdot \nu = j \cdot \nu = j_{in} \cdot \nu \quad \text{on } \Sigma^* := \Sigma \setminus \cup_{i=1}^{\mathcal{N}} \partial C^{(i)}, \tag{8}$$

at the gas/solid interface we may assume due to catalyst coverage

$$-\nabla c_l \cdot \nu = 0 \quad \text{on } \Sigma \setminus \overline{\Sigma^*}. \tag{9}$$

We may expect that j_{in} is periodically at the electrode surface, consisting alternatingly of platinum (catalyzes hydrogen reduction reaction) and glass (no hydrogen production), and being zero close to surface caps. We recall that nucleation is not considered in the model, only at the electrode boundary Σ^*, where no caps cover the surface, a steady flux of hydrogen enters. Furthermore, we do not model the detachment of surface nanobubbles that might become spherical nanobubbles subsequently. By symmetry, we assume no flux conditions on the side boundaries

$$-\nabla c_l \cdot \nu = 0 \quad \text{on } \Pi, \tag{10}$$

and a constant hydrogen outflux on the top boundary

$$-D_l\nabla c_l \cdot \nu = j_{out} \cdot \nu \quad \text{on } Z, \tag{11}$$

in order to model a static flux of hydrogen ions (protons) in direction of the anode of the fuel cell, passing through the membrane on its further way.

3.2 Many bubbles problem and scaling

In principle we have to solve for c_l the Laplace equation following from (3)

$$\Delta c_l = 0 \quad \text{in } L \tag{12}$$

combined with the b.c. $(6)_2$ for each index i and (8)–(11). In G, the concentrations $c_g^{(i)}$ within each bubble are constant and given by the respective formula $(6)_1$. This allows to simplify the radii evolutions (7), to

$$\frac{\partial}{\partial t}\mathcal{R}^{(i)} = -D_l\frac{\nabla c_l^{(i)} \cdot \nu}{c_l^{(i)} - c_g^{(i)}} \quad \forall i = 1, \ldots, \mathcal{N}. \tag{13}$$

This is complemented by the above mentioned initial conditions for $\mathcal{N}, \mathcal{N}_s$, and $\mathcal{R}^{(i)}$, $i = 1, \ldots, \mathcal{N}^0$. Our many bubbles problem is a generalization of the classical Mullins-Sekerka model by introducing nanocaps and a different Stefan condition.

We assume that typical distances between bubbles are larger than their radii and widths, such that within the considered time interval the effect of intersecting bubbles may be safely neglected. A typical radius $\mathcal{R}$ is of the order of several nanometers, while the typical distance between nanobubbles is about ℓ, i.e. a micrometer. In order to emphasize the different scales in the equations we introduce a scaling factor $\hat{\varepsilon} = 10^{-1}$. We extend Q formally by adding periodically $\mathcal{N}^0 - 1$ boxes, parallel to the electrode surface plane. Radii and radii of curvature, relevant for the single bubble solutions scale with $\mathcal{R} = \hat{\varepsilon}\ell$, $\ell \sim \varepsilon$, while the number $\mathcal{N}^0$ of nanobubbles scales with ε^{-2}. Note that bubble volumes scale therefore with $\hat{\varepsilon}^3 = 10^{-3}$. In order

to balance (6) we scale $\gamma \sim \mathcal{R}$. Diffusion times scale as $(\mathcal{N}^0)^2$. The capacity of all bubbles goes with $\hat{\epsilon}\,\ell\,\mathcal{N}^0$, we set $\hat{\varepsilon} = \varepsilon^2$ for a dilute regime. Within this scaling regime, we see (Niethammer et al. (2001)) that the solution c in the neighbourhood of a bubble is basically the solution for this single bubble problem alone, approaching the "mean field" concentration $\overline{c}$ for an infinite radius. It turns out that this so-called mean field approach allows to solve our many bubbles problem efficiently. The solution of the full problem for c_l would require the numerical solution of a PDE with many free boundaries, requiring finite element methods for a time-dependent domain, while in our approach only one ODE for $\overline{c}$ has to be solved instead. We use same notations in the scaled case from now on.

3.3 Single bubble problem

For a single nanosphere alone, we solve (12) on $\mathbb{R}^3 \setminus B_{\mathcal{R}^{(i)}}(X^{(i)})$ together with $\lim_{r\to\infty} c = \overline{c}$, $r = |x - X^{(i)}|$, and $(6)_2$ as b.c. Note that $\overline{c}$ depends on time only and might be interpreted as a concentration far away from any kind of bubbles. The problem is spherical symmetric and the solution denoted by $\tilde{c}_l^{(i)}$ is obtained by the well-known fundamental solution for the Laplace operator,

$$\tilde{c}_l^{(i)}(r) = (c_l^{(i)} - \overline{c})\hat{\varepsilon}\mathcal{R}^{(i)}/r + \overline{c}. \tag{14}$$

For the Stefan condition (13), by means of

$$\frac{\partial}{\partial r}\tilde{c}_l^{(i)}(\hat{\varepsilon}\mathcal{R}^{(i)}) = -(c_l^{(i)} - \overline{c})/(\hat{\varepsilon}\mathcal{R}^{(i)}), \tag{15}$$

we get for the scaled evolution of $I^{(i)}$

$$\frac{\partial}{\partial t}\mathcal{R}^{(i)} = \frac{D_l}{\mathcal{R}^{(i)}}\frac{c_l^{(i)} - \overline{c}}{c_l^{(i)} - c_g^{(i)}}. \tag{16}$$

The radial symmetry applies to spherical nanocaps as well. Solving (12) on $\{x \in \mathbb{R}^3 \setminus B_{\mathcal{R}^{(i)}}(X^{(i)}) \,|\, x_3 > 0\}$ similar as for a single sphere yields (14), too. We have to guarantee the b.c. on Σ^*

$$\nabla\tilde{c}_l^{(i)}|_{\Sigma^*}(r)\cdot\nu \stackrel{!}{=} j_{in}\cdot\nu. \tag{17}$$

Due to radial symmetry the left hand-side is zero, thus we may consider in this case only $j_{in} = 0$. We recall that close to surface caps, we have assumed $j_{in} = 0$. W.l.o.g. we may adapt for j_{in}, that is not zero everywhere, by adding a suitable global "background" term to $\tilde{c}_l^{(i)}$, but this would give rise to technical issues with the assumption that $c_l^{(i)}$ is constant on $I^{(i)}$. Since this background term does not dominate the radii evolution, we omit it here. We encounter the same form of Stefan condition (16) as for a single spherical nanobubble.

3.4 Mean field model

In order to solve the many bubbles problem, we construct a formal macroscopic solution with $\check{c}_l^i = \mathcal{N}^0\tilde{c}_l^i - (\mathcal{N}^0 - 1)\overline{c}$

$$c_\infty(x) = \frac{1}{\mathcal{N}^0}\sum\nolimits_{i=1}^{\mathcal{N}_s}\check{c}_l^{(i)}(x) + \frac{1}{\mathcal{N}^0}\sum\nolimits_{i=\mathcal{N}_s+1}^{\mathcal{N}_s+\mathcal{N}_c}\check{c}_l^{(i)}(x). \tag{18}$$

Clearly $\Delta c_\infty = 0$ in $\{x \in \mathbb{R}^3\setminus\overline{G} \,|\, x_3 > 0\}$. If we let formally $\varepsilon \to 0$ for the moment and $\mathcal{N}/\mathcal{N}^0 \approx 1$, this would yield $\{x \in \mathbb{R}^3 \,|\, x_3 > 0\}$

$$\lim_{\varepsilon\to 0} c_\infty \approx c_l^{(i)} \quad \text{if } |x - X^{(i)}| - \hat{\varepsilon}\mathcal{R}^{(i)} \to 0 \text{ for some } i, \tag{19}$$

$$\lim_{\varepsilon\to 0} c_\infty \approx \overline{c} \qquad \text{otherwise.} \tag{20}$$

Thus we may assume that the global solution c of the many bubbles problem is well approximated by a superposition of the single bubble problem solutions $\tilde{c}_l^{(i)}$. The free boundary condition (16) for the radii of spheres and caps does not depend on ε, and may be rewritten as

$$\frac{\partial}{\partial t}\mathcal{R}^{(i)} = -\frac{D_l}{\mathcal{R}^{(i)}}\frac{H}{1-H}\left(1 - \mathcal{R}^{(i)}\frac{\overline{c}}{\sigma}\right). \tag{21}$$

In order to determine the mean field concentration $\overline{c}$ we consider the global hydrogen balance over a total time $\mathcal{T}$. For a quasi-static equilibrium, we assume a total zero net flux and outflux into the considered domain Q, i.e.

$$J_{tot} := \int_0^{\mathcal{T}}\left(\int_\Sigma j_{in}\,dA + \int_Z j_{out}\,dA\right)dt = 0 \tag{22}$$

s.t. the initial amount $C_0 = \hat{c}_l|Q|$ of hydrogen in the box Q is conserved:

$$\int_L \overline{c}\,dV + \sum_{i=1}^{\mathcal{N}}\int_{G^{(i)}} c_g^i\,dV = C_0 + J_{tot} = C_0. \tag{23}$$

Using that $\overline{c}$ depends on time only and $(6)_2$, we get as first-order expansion in ε (the zero-order yields only $\overline{c} = \hat{c}_l$)

$$\left(|Q| - \frac{4\pi}{3}\frac{\varepsilon^3}{\mathcal{N}^0}\left(\sum_{i=1}^{\mathcal{N}_s}(\mathcal{R}^{(i)})^3 + \sum_{i=\mathcal{N}_s+1}^{\mathcal{N}}\omega(\mathcal{R}^{(i)})^3\right)\right)\overline{c}$$
$$+ \frac{4\pi}{3}\frac{\varepsilon^3\sigma}{\mathcal{N}^0 H}\left(\sum_{i=1}^{\mathcal{N}_s}(\mathcal{R}^{(i)})^2 + \sum_{i=\mathcal{N}_s+1}^{\mathcal{N}}\omega\,(\mathcal{R}^{(i)})^2\right) = C_0. \tag{24}$$

We end up with

$$\overline{c} = \frac{\hat{c}_l - \frac{4\pi}{3}\frac{\varepsilon^3}{\mathcal{N}^0|Q|}\frac{\sigma}{H}\sum_{i=1}^{\mathcal{N}}\omega^{\chi(i)}(\mathcal{R}^{(i)})^2}{1 - \frac{4\pi}{3}\frac{\varepsilon^3}{\mathcal{N}^0|Q|}\sum_{i=1}^{\mathcal{N}}\omega^{\chi(i)}(\mathcal{R}^{(i)})^3}, \tag{25}$$

where $\chi(i) = 1$ if $\mathcal{N}_s + 1 \le i \le \mathcal{N}$ and $= 0$ otherwise. Due to the ansatz of a quasi-static in-/outflux there is no effect due to the partial coverage of Pt at the electrode by hydrogen surface caps. Since a concentration should be non-negative, our model breaks down when $\overline{c} < 0$ corresponding to too large bubbles that might intersect. The latter being a contradiction to our scaling assumptions in Subsect. 3.2. However, for consistent initial radii, we may expect that for a sufficiently small time $\mathcal{T} > 0$ the constraint $\overline{c} \ge 0$ is guaranteed.

For a rigorous derivation of the macroscopic LSW equations from the classical Mullins-Sekerka model in the limit $\varepsilon \to 0$ see Niethammer et al. (2001). We assume that there exists only a finite initial number of different radii, that recur periodically over the infinite number of boxes Q. Inserting in the LSW equations as initial data a finite sum of Dirac distributions corresponds to a finite number of different radii initially, as in our situation. This motivates our mean field model, for a positive but small ε.

We solve the ordinary differential equations (21), completed with initial conditions, and the algebraic equation (25) until for the first time $\tau^{(j)}$ a bubble vanishes, i.e. $\tau^{(j)} := \inf_{t\in[0,\mathcal{T}]}\{\mathcal{R}^{(j)}(t) \le 0\}$ for some j. Then we take out bubble j by fixing $\mathcal{R}^{(j)} = 0$ for all times $t > \tau^{(j)}$ and restart solving our differential algebraic equation (DAE) system on $[\tau^{(j)}, \mathcal{T}]$ with new initial conditions $\mathcal{R}^{(i)}(\tau^{(j)}+) = \mathcal{R}^{(j)}(\tau^{(i)}-)$ for all $i \ne j$. We proceed until the next bubble dissolves or until the maximal time $\mathcal{T}$ is reached.

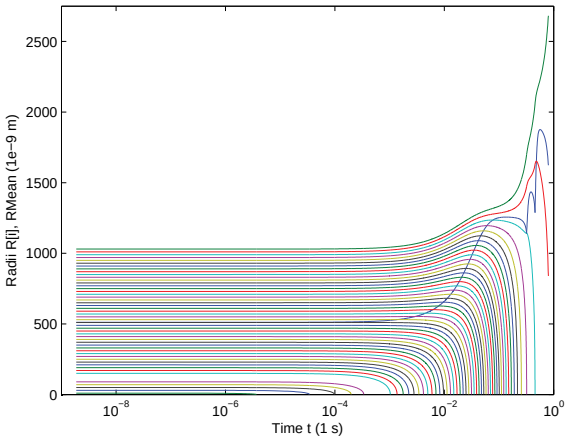

Fig. 2. Time evolution of 50 curvature radii up to $\mathcal{T} = 0.2\,\mathrm{s}$ with a logarithmic time scale. The 5 smaller radii ($\mathcal{R}_0^{(i)} = 10 - 90$ nm) are associated with nanospheres, the other with nanocaps ($\mathcal{R}_0^{(i)} = 150 - 1030$ nm). The mean field $\overline{\mathcal{R}}$ is depicted in darkblue.

3.5 Numerical simulations

The DAE system, described in the last subsection, has index 1. We differentiate (25) w.r.t. time and solve by Matlab using the solver ode113. This approach is applied, since solving the DAE directly by means of suitable Matlab solvers, like ode15s or ode23t, exhibits problems at the points $\tau^{(j)}$ in time, when droplets vanish. We assume a supersaturation concentration $\hat{c}_l = 5.0\,\mathrm{mol/m^3}$, for the other underlying data see table 1. For ease of presentation we represent the mean field concentration by a corresponding radius value,

$$\overline{\mathcal{R}} := \sigma \,/\, \overline{c} \tag{26}$$

motivated by $(6)_2$ and (21). We emphasize that $\overline{c}$ being a concentration is non-negative.
For the radii evolution, where the mean field is represented by an equivalent radius (26), see Fig. 2. We see that with exception of the largest bubbles all precipitates disappear, in particular all spheres dissolve. However, we observe several meta-stable bubble radii, corresponding to caps, for times of $10^{-3} - 10^{-1}$s. This corresponds to the experimental observations described above and validates our model. Furthermore, $\overline{\mathcal{R}}$ approaches the meta-stable states $\mathcal{N}/(\sum_{i=1}^{\mathcal{N}} \omega^{\chi(i)}/\mathcal{R}^{(i)})$ until a droplet vanishes.

Stationary solutions. We consider possible stationary solutions. We recall that we have already assumed the quasi-static partial differential equation (12) and the quasi-static Henry's law (5). From the Stefan conditions (21) we get directly that $\mathcal{R}^{(i)} = \overline{\mathcal{R}}$ has to hold for all bubbles i, existing at time t. Trivially, the mean field $\overline{c}$ is then stationary, i.e. constant in time. We exploit (25) in this case in order to calculate possible stationary radii $\mathcal{R}_\infty$,

$$\frac{\sigma}{\mathcal{R}_\infty} = \hat{c}_l + \frac{4\pi\sigma\varepsilon^3}{3\mathcal{N}^0|Q|}\left(\mathcal{N}_s + \mathcal{N}_c\,\omega\right)\frac{1-H}{H}\mathcal{R}_\infty^2. \tag{27}$$

We assume that at least one bubble remains, i.e. $\mathcal{N}^\infty > 0$. Let $\xi := \mathcal{N}_s^0/\mathcal{N}^0 \in [0,1]$ denote the percentage of the initial number of spheres w.r.t. the number of all bubbles for a stationary solution and let $\eta_s = \varepsilon^3\mathcal{N}_s^\infty/\mathcal{N}^\infty, \eta_c = \varepsilon^3\mathcal{N}_c^\infty/\mathcal{N}^\infty \in [0,1]$ denote the stationary fraction of nanospheres and nanocaps, then

$$\mathcal{R}_\infty^3 - (\hat{c}_l/\sigma)\Xi\mathcal{R}_\infty + \Xi = 0, \tag{28}$$

where $\Xi := 3|Q|H/(4\pi(1-H)(\eta_s\xi + \eta_c(1-\xi)\omega)$. A cubic polynomial in $\mathcal{R}_\infty$ as the l.h.s. of (28) has a unique non-negative minimum at $\sqrt{\hat{c}_l\Xi/(3\sigma)} > 0$. The minimum value is negative, yielding two stationary radii, iff $\hat{c}_l > 3\sigma(4/\Xi)^{1/3}$ which is clearly fulfilled for our data for all ξ, η_s, and η_c. In case of equality in the latter condition we would have one stationary radius, otherwise there is none. In the case $\xi = 0.1$, i.e. as many caps as spheres, and $\eta_s = 0$, $\eta_c = 1/50$ (no spheres persist but 1 of the initial caps remains), we find numerically $\mathcal{R}_\infty \approx 220.0$ nm and $2.942 \cdot 10^{10}$m (that is irrelevant). The first solution corresponding to the stationary surface cap width $a_\infty = 19.17$ nm. A comparison with table 1 shows that this value is within the range of typically widths. Equivalently for the stationary mean field concentration follows $\overline{c}_\infty = \sigma/\mathcal{R}_\infty \approx 5.0\,\mathrm{mol/m^3}$. Neither varying ξ, η_s, η_c nor Θ has a significant effect on the smaller stationary value.
As we will discuss in the next section for our second example, the smaller stationary radius is unstable. Only the situation of no bubble is stable. The situation might be different when the dynamic equilibrium is taken into account as in Sperre (2014) or when water vapour in the bubbles is considered, too.

4. NANODROPLETS IN THE HEAT TREATMENT OF GALLIUM ARSENIDE WAVERS

A mathematically similar mean field model is proposed in Kimmerle (2009) within the context of precipitation of liquid As rich droplets in GaAs crystals, as described in Sect. 1. This application is different to the hydrogen bubbles in the sense that the precipitates consist of two substances, As and Ga, we work with a parabolic equation, and $\mathcal{N}^0 \sim \varepsilon^{-3}$. For thermodynamic consistency the considered convex domain Q has to be time-dependent, too. It is natural for this problem to work with the total chemical potential u instead of a concentration c as in the hydrogen electrolysis model. u_l is a general form of a Dirichlet b.c. like $(6)_2$ on the interface. Furthermore, $\tilde{\mathbb{X}}$ and $\mathcal{X}$ are given functions modelling inter alia jumps of the As and Ga concentrations at the interface. In the DC regime we have for the radii and the mean field of the chemical potential

$$\frac{\partial}{\partial t}\mathcal{R}^{(i)} = \frac{\overline{u} - u_l(\mathcal{R}^{(i)})}{\mathcal{R}^{(i)}\tilde{\mathbb{X}}(\mathcal{R}^{(i)})} \quad \forall i \in \{1,\dots,\mathcal{N}\}, \tag{29}$$

$$\frac{\partial}{\partial t}\overline{u} = -4\pi\frac{\frac{1}{\mathcal{N}^0}\sum_{i=1}^{\mathcal{N}}\mathcal{R}^{(i)}(\overline{u} - u_l(\mathcal{R}^{(i)}))}{\mathcal{X}(\overline{u})\,|Q|}, \tag{30}$$

with initial conditions $\mathcal{R}^{(i)}(0) = \mathcal{R}_0^{(i)}$, for all $i \in \{1,\dots,\mathcal{N}^0\}$, $\overline{u}(0) = \overline{u}_0$. The latter initial value has to be computed consistently from an algebraic equation for $\overline{u}$ that follows analogously as above from a conservation law (here for As). For the time-dependent domain Q we use the equation from total conservation of mass.

4.1 Stability of a finite number of liquid droplets

For the material data and further details, we refer to Kimmerle (2009). Let N_0, M_0 denote the total amount

of As and total mass, c_l, c_s denote the As concentration in the liquid droplets and in the solid crystal, resp., $\hat{c}_s$ the prescribed total concentration. The total number of atoms in the droplet is n_l. ρ_l and ρ_s are the mass densities in liquid and solid. Again $\mathcal{R}_\infty$ denotes a stationary radius, while $\eta_\infty = \mathcal{N}_\infty/\mathcal{N}_0$ is the stationary precipitate fraction.

Lemma 1. (Necessary & sufficient stationarity conditions). 1) We have stationary solutions with $\mathcal{N}^\infty \in \{1, \dots, \mathcal{N}^0\}$ droplets, iff

$$\mathcal{R}^{(i)} = u_l^{-1}(\overline{u}_\infty) =: \mathcal{R}_\infty \quad \forall i \in \{1, \dots \mathcal{N}\}, \tag{31}$$

$$\overline{u}_\infty = c_s^{-1}\left(\frac{N_0\hat{c}_s - \frac{4\pi}{3}\eta_\infty \mathcal{R}_\infty^3 c_l(\mathcal{R}_\infty) n_l(\mathcal{R}_\infty)}{N_0 - \frac{4\pi}{3}\eta_\infty \mathcal{R}_\infty^3 n_l(\mathcal{R}_\infty)}\right), \tag{32}$$

$$|Q_\infty| = \frac{M_0 - \frac{4\pi}{3}\eta_\infty \mathcal{R}_\infty^3 \rho_l(\mathcal{R}_\infty)}{\rho_s(\overline{u}_\infty)} + \frac{4\pi}{3}\eta_\infty \mathcal{R}_\infty^3. \tag{33}$$

2) If we assume that $\overline{u}_\infty$ is concave as function of $\mathcal{R}_\infty$, if we assume that u_l is convex in $\mathcal{R}^{(i)}$ and if $\lim_{r\to\infty} c_s(u_l(r)) < \hat{c}_s$, then (31) has two solutions for the stationary radius $\mathcal{R}_\infty$ for sufficiently large N_0.
3) In the special case $\mathcal{N}^\infty = 0$ we have equilibria iff $\overline{u}_\infty = c_s^{-1}(\hat{c}_s)$ and $|Q_\infty| = M_0/\rho_s(\overline{u}_\infty)$.

In the next theorem we use instability, asymptotic stability and stability as defined in Walter (1998).

Theorem 2. (Stability of stationary mean field solutions). We consider a fixed number $\mathcal{N}^\infty$ of stationary droplets.
(i) The smaller of the two radii $\mathcal{R}_\infty$ are always unstable ("critical radius").
(ii) The larger stationary radii are unstable for $\mathcal{N}^\infty > 1$ and asymptotically stable for $\mathcal{N}^\infty = 1$.
(iii) For $\mathcal{N}^\infty = 0$ the system is stable, but not asymptotically stable.

For proofs we refer to (Kimmerle, 2009, Lemma 6.3, Th. 6.1). The latter result uses the Poincaré-Lyapunov theorem Walter (1998), linearizing around stationary solutions.

5. CONCLUSION AND OUTLOOK

For hydrogen electrolysis, we have proposed a new model for the evolution of precipitates within the process. Our model incorporates spherical and cap-like surface nanobubbles and provides an explanation for their long lifetimes. Contrary to Sperre (2014), who considers only one flat surface nanocap in case of a dynamic equilibrium, we have considered the quasi-static equilibrium of many bubbles, but without a flat bubble assumption. It might be interesting to model the evolution of the contact angles $\Theta^{(i)}$, too, but since only $\cos(\Theta^{(i)})$ enters in the dynamics in ω, we shall not expect large effects for small contact angles.
One of the next tasks will be the incorporation of micropancakes or possible other forms of microfilms. The relation between micropancakes and surface nanobubbles is not completely understood so far.
Another open question is whether fast transportation phenomena near the electrode/electrolyte interface, that have been observed experimentally by Guiterres et al. (2007), are relevant for our model. A extension would be to follow Ward et al. (1970), who propose a model for a multiphase bubble, e.g. vapour could be present in our case. This approach might yield further stationary radii, different stability, and an explanation for nucleation by the existence of a critical radius. Moreover, this new Mullins-Sekerka model for spheres and caps exhibits an interesting interplay between the different types of bubbles. Once our model has been elaborated further, the next step will be the optimization of the hydrogen electrolysis. For optimal control of a macroscopic model for phase transitions, see Kimmerle (2013).
The results on stationary radii and its stability may be extended from As-rich droplets in GaAs to the hydrogen nanobubbles. Note that the results of the GaAs model fit well to experimental observations, see Dreyer et al. (2008) as well as the numerical simulations (qualitatively similar to the first example) in Kimmerle (2009).

ACKNOWLEDGEMENTS

S.-J. K. would like to express his sincere thanks to Peter Berg at NTNU for pointing out this interesting problem (Sperre (2014)) to him and for valuable comments.

REFERENCES

P. Berg, S.-J. Kimmerle, and A. Novruzi. Modeling, shape analysis and computation of the equilibrium pore shape near a PEM-PEM intersection. *Journal of Mathematical Analysis and Applications*, 410:241–256, 2014.

W. Dreyer, and F. Duderstadt, F. On the modelling of semi-insulating GaAs including surface tension and bulk stresses. Proc. Roy. Soc. London Ser. A, 464:2693–2720, 2008.

A.C. Guiterres, A.L.N. Pinheiro, T. Iwasita, and W. Vielstich. New mechanism of gas transport at the interface solid/liquid. *Electrochim. Acta*, 52:2317-2321, 2007.

S.-J. Kimmerle. *Macroscopic diffusion models for precipitation in crystalline gallium arsenide - Modelling, analysis and simulation.* PhD thesis. Humboldt-Universitt zu Berlin, Berlin, 2009.

S.-J. Kimmerle. Optimal control of mean field models for phase transitions. In I. Troch, F. Breitenecker, editors, *7th Vienna International Conference on Mathematical Modelling, Vienna, Austria, February 14–17, 2012; IFAC Mathematical Modelling*, volume 7/1, pages 1107–1111, 2013.

L. Luo, and H.S. White. Electrogeneration of single nanobubbles at sub-50-nm-radius platinum nanodisk electrodes. *Langmuir*, 29:11169–11175, 2013.

B. Niethammer, and F. Otto. Ostwald Ripening: The screening length revisited. *Calc. Var. Partial Differential Equations*, 13:33–68, 2001.

J.R.T. Seddon, D. Lohse, W.A. Ducker, and V.S.J. Craig. A deliberation on nanobubbles at surfaces and in bulk. *Chem. Phys. Chem.*, 13:2179–2187, 2012.

A.H. Sperre. *Modeling surface nanobubbles in water electrolysis.* Specialization project report. Department of Physics, NTNU, Trondheim, Norway, 2014.

W. Walter. *Ordinary Differential Equations* Springer, New York, 1998.

C.A. Ward, A. Balakrishnan, and F.C. Hooper. On the thermodynamics of nucleation in weak gas-liquid solutions. *J. Basic Eng.*, 92:695–701, 1970.

X.H. Zhang, A. Quinn, and W.A. Ducker. Nanobubbles at the interface between water and a hydrophobic solid. *Langmuir*, 24:4756–4764, 2008.